Investigation of Jet Curtains for Chemical Laser Application

S. Boraas*
Bell Aerospace Textron, Buffalo, N.Y.

A method is presented for passively containing reacting gas within the cavity of a chemical laser using a combination of cavity wall displacement and jet curtains. Suggesting several advantages over the matched pressure approach, the concept was evaluated in an application to a DF laser using the hydraulic analogy. Analyses were made to determine the flow characteristics of the confined and unconfined laser gas, the jet curtain requirements, and basic information for the design of the test hardware (water table). Experiments were conducted on the water table with the jet nozzle size, jet exit Froude number, and wall displacement as the variables. The results of these experiments qualitatively demonstrated the feasibility of the containment concept and demonstrated that for a given nozzle size, the ideal wall displacement is that which requires the minimum jet Froude number for containment.

Introduction

IN a chemical laser, the power is extracted from the cavity in a transverse direction to the gas flow. This means that the optical system requires apertures in the cavity walls and that these be located downstream of the entrance to the cavity and sized to approximately span the lasing zone. The heat release within the lasing zone will generate a static pressure rise which, when combined with the aspirating effect of the flow across the apertures, will result in a transverse pressure gradient and a lateral expansion of the laser gas. Some of this gas will enter the tunnels leading to the mirror cavities and may reach and contaminate the mirror surfaces unless measures are taken to prevent it.

Reference 1 describes a method of preventing the laser gas from entering the tunnel by injecting a noncontaminating gas into the mirror cavity and thereby increasing the flow static pressure there to a point where it matches the laser gas static pressure at the aperture. This is referred to as "matched pressure" injection. This paper discusses a recently completed study of a more passive method of gas containment in which an aerodynamic barrier is used much in the same manner as described in Ref. 2. In this concept, the gas is permitted to expand freely in the lateral direction, and its capture is achieved by a lateral displacement of the cavity sidewalls. In addition, a constant Mach number inert gas jet located at each aperture and flowing across it in the direction of the laser gas serves as a barrier or curtain to prevent the latter's entrance into the mirror cavities. When wall displacement is sufficient to capture the laser gas plus a major portion of the flow from the jets, while diverting the remainder into the mirror cavity, then this containment concept exhibits the following desirable features:

1) Capturing the expanded gas rather than forcibly containing the unexpanded gas eliminates the introduction of shock disturbances in the lasing zone.

2) The placement of the coflowing jet adjacent to the laser gas when coupled with an adequate wall displacement will prevent the formation of a large zone of recirculating laser gas at the tunnel entrance as a result of the latter's partial entrance into the tunnel. Such a recirculation can bring harmful deactivants back to the start of the lasing zone.

3) The coflowing nature of the jet minimizes its disturbance impact upon the laser gas compared with jets used to replenish the mirror cavities for matched pressure injection.

4) By using a relatively low-temperature gas in the jet, the portion which is captured will act not only as an ingestion barrier but also as an insulation to reduce heating of the cavity wall as a result of laser gas impingement and reattachment.

5) Deflection of the uncaptured portion into the mirror cavities will offset the aspiration effect and thereby avoid the need for gas replenishment within the cavities.

The purpose of the study was to determine the feasibility of this concept by evaluating its application in a DF laser using the hydraulic analogy. It was divided into two phases, the analytical and the experimental. Although qualitative, the experimental results confirmed the feasibility of the concept. A discussion of this study is given in the subsequent sections.

Analyses

A major segment of the study was a four-part analytical phase conducted preparatory to conducting the experimental phase. The first part investigated the laser gas and consisted of an analysis to determine the flow properties of the confined gas and an estimate of its expansion and diffusion across the apertures. The second examined the jet curtain requirements. The third reviewed the hydraulic analogy and its application to this particular problem. Finally, the last part involved development of basic design information for the test hardware.

Laser Gas

The properties of the confined gas within the laser cavity were calculated for a specific set of nozzle exit bank conditions and the cavity contour shown in Fig. 1. Then the lateral expansion and diffusion of the laser gas across the aperture was estimated assuming a tunnel pressure equal to the nozzle exit plane pressure.

Confined

The basic analysis involved the confined gas. Figure 1 shows a diagram of the DF laser being considered. The 2.66×15.24-cm nozzle bank consists of multiple two-dimensional alternating D_2 and F_2 nozzles. The sidewalls of the laser cavity are parallel to the x axis and the half-angle of the top and bottom walls is 7.8 deg. The dashed outlines on the sidewalls are the aperture locations (when present) and denote the intersection of the mirror tunnel walls with the cavity sidewalls.

The flow from any two adjacent nozzles mixes and chemically reacts upon entering the laser cavity. The resultant heat release changes the pressure, temperature, and Mach number of the confined gas. Axial and normal (z direction) variations in these as well as other properties of the gas

Received May 6, 1977; revision received Oct. 4, 1977.

Index categories: Lasers; Hydrodynamics.

*High Energy Laser Technology. Member AIAA.

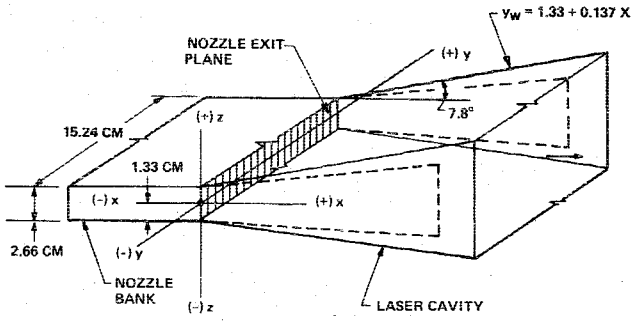

Fig. 1 Schematic of a DF laser.

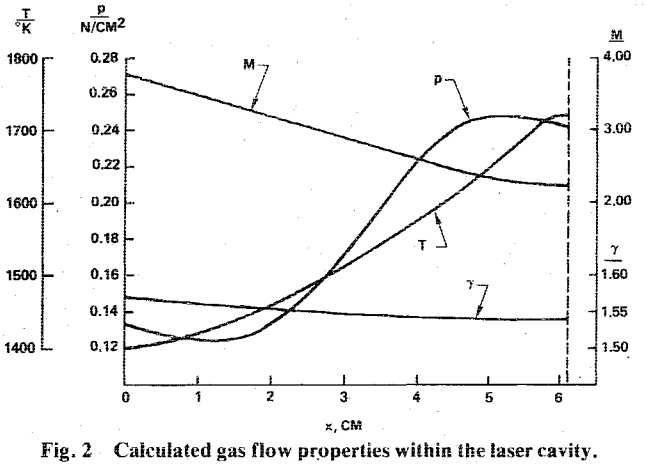

Fig. 2 Calculated gas flow properties within the laser cavity.

depend upon the rate of heat release which, in turn, depends upon the mixing model employed. In this study, this flow was analyzed using the BLAZE-IV[3] computer program. This program, which was formulated from the three-dimensional conservation equations, accounts for normal pressure gradients, since the normal momentum equation was retained in its development. The code contains a finite rate chemical kinetics model and permits the use of several mixing models.

The flowfield within the laser cavity was analyzed for the following values of gas total temperature, Mach number, static pressure, specific heat ratio, and molecular weight at the nozzle exit plane: $T_e = 1400.0$ K, $M_e = 3.8$, $p_e = 0.133$ N/cm^2, $\gamma_e = 1.57$, $W_e = 8.12$. Calculated values of the first four of these quantities were mass weighted in the normal direction, at each axial station, to obtain values along the plane of symmetry (x,y plane of Fig. 1). These values, which are plotted in Fig. 2, show that the total temperature reaches a constant maximum value at a distance of about 6.1 cm downstream of the nozzle exit plane. This 6.1-cm heat addition region is the zone of gas lasing, which means that for complete power extraction the apertures must have at least this width. In the present configuration, the apertures were 7.62 cm.

The results of Fig. 2 were required in analytical form for subsequent calculations. With x expressed in centimeters, these expressions are

$$T = 1400.0 + 14.33x + 9.25x^2 - 0.46x^3 \text{ (K)} \quad (1)$$

$$M = 3.8 - 0.29x \quad (2)$$

$$\gamma = 1.57 - 0.007x \quad (3)$$

$$p = 0.133 - 0.002x \text{ (N/cm}^2\text{)} \quad (0 < x \leq 1.5) \quad (4a)$$

$$p = 0.078 + 0.035x \text{ (N/cm}^2\text{)} \quad (1.5 < x \leq 5.1) \quad (4b)$$

$$p = 0.266 - 0.002x \text{ (N/cm}^2\text{)} \quad (5.1 < x \leq 6.1) \quad (4c)$$

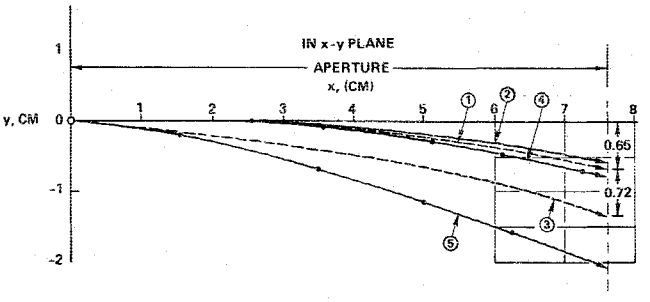

CURVE	DESCRIPTION	FLUID	γ	PRESSURE CONDITION
①	CALC.STREAMLINE	GAS	VAR	$p_t = p_e$
②	CALC.STREAMLINE	WATER	2.0	$p_t = p_e$
③	EST.OUTER BOUNDARY	GAS	CONST	$p_t = p_e$
④	MEAS.STREAMLINE	WATER	2.0	$p_t \cong p_e$
⑤	MEAS.OUTER BOUNDARY	WATER	2.0	$p_t < p_e$

Fig. 3 Laser gas streamline and outer boundary across the aperture.

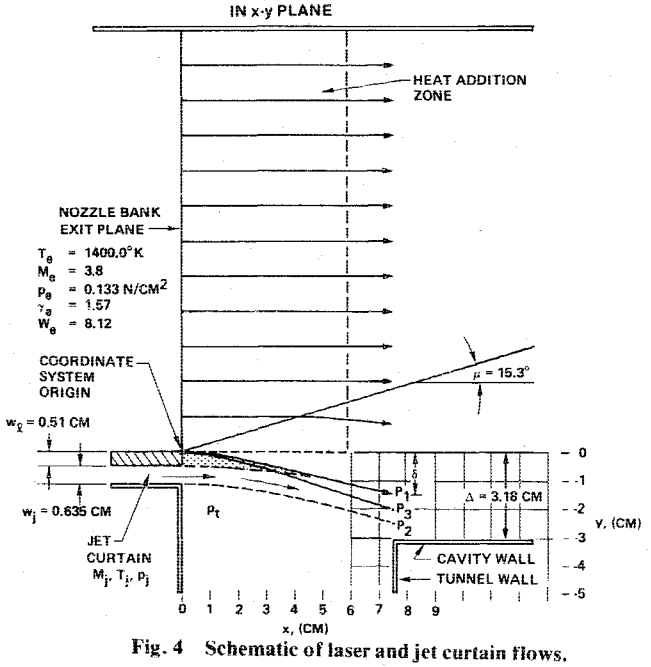

Fig. 4 Schematic of laser and jet curtain flows.

Unconfined

The increase in static pressure of the laser gas is the driving force in its lateral expansion. From Fig. 2, it is seen that this rise occurs approximately between $x = 1.5$ cm and $x = 5.1$ cm. For values of $x < 1.5$ cm the pressure is relatively constant at a value near that at the nozzle exit plane and for values of $x > 5.1$ cm, the pressure is again nearly constant at a value which is about twice that at the exit plane. One would therefore expect that, if the optical system were attached to the cavity of the laser shown in Fig. 1 and if the static pressure (p_t) at the tunnel entrance to optical system were equal to that at the nozzle exit plane, then the lateral expansion of the laser gas would start near $x = 1.5$ cm increase at an increasing rate up to $x = 5.1$ cm, and then expand at a nearly constant rate for $x > 5.1$ cm. These were the assumptions made in the calculations of the outer streamline of the expanding gas.

In determining the outer streamline contour, the confined gas was treated as being locally isentropic. That is, at every station x, the confined gas was assumed to exhibit flow properties consistent with Eqs. (1-4). The outer streamline was then assumed to be the locus of points representing the accumulative effect of a Prandtl-Meyer expansion from each of several stations along the x direction under the condition that $p_t = p_e$. This outer streamline as it appears across the

aperture is shown by curve 1 in Fig. 3 along with another streamline, curve 2, computed from the same set of properties in Eqs. (1, 2, and 4) but with a constant value of $\gamma = 2$. As will be shown later, the latter represents the streamline when water rather than gas is the expanding medium.

Based upon the results of Fig. 3, the present optical system with its 7.62-cm apertures would require a wall displacement of 0.65 cm just to capture the laser gas, providing that $p_t = p_e$. In practice this will not be the case because the aspirating effect of the high-speed laser gas on the gas within the tunnel will substantially lower p_t, thereby causing a greater expansion than indicated in Fig. 3. Nevertheless, these results suggest what the lower limit of wall displacement must be if containment of the gas is to be realized.

Figure 4 is a schematic showing the optical system attached to the laser. The view is in the xy plane and shows the jet and optical tunnel on only one side of the laser cavity since identical conditions would exist on the opposite side. The schematic also shows the location of the heat addition zone relative to the aperture and the cavity wall as being displaced an amount Δ relative to the x axis. The Mach angle of the laser gas at the nozzle exit plane is $\mu = \sin^{-1}(1/M_e) = 15.3$ deg, so that the portion of the laser gas which will experience a lateral expansion lies within the corner Mach cone whose half-angle is 15.3 deg.

The outer gas streamline is shown to pass through point P_1 at the downstream end of the aperture. Its deflection δ, although unknown at this point, is known to be larger than the value of 0.65 cm shown in Fig. 3 since aspiration effects make $p_t < p_e$. Points P_1 and P_2 represent the outer boundaries (dashed lines) of the jet at the same axial location. The placement of the jet next to the nozzle bank results in a flow region (shaded area) downstream of the land which is aspirated by both the laser gas and the jet. This has an additional effect of causing the laser gas to start expanding prior to the $x = 1.5$ cm point downstream of the nozzle exit plane.

Jet Curtain Requirements

An analysis of the jet impingement upon the expanding laser gas as shown in Fig. 4 revealed that when the jet exit pressure p_j equals the tunnel pressure, a jet with an arbitrarily selected width w_j of 1.27 cm will not disturb the expanding laser gas within the corner Mach cone. This was found to be true for all jet Mach numbers M_j. One concludes from this that jets with $w_j < 1.27$ cm would also be acceptable as far as a laser gas flow disturbance is concerned. However, an important factor in the selection of the jet width is the viscous effects of the tunnel and laser gas on the jet as it traverses the aperture; if the width is not sufficient, the jet can be so eroded by diffusion as to make it totally ineffective.

The jet as it enters the tunnel will be turbulent and will have a constant velocity distribution. Velocity discontinuities will exist at the interfaces of the jet with the gases on either side of it immediately downstream of the entrance point. The smoothing of these discontinuities as a result of turbulent mixing is discussed by Schlichting.[4] If the velocity of the gas in the tunnel is assumed to be essentially zero, then from this reference an experimentally determined value for the semiwidth of the mixing region involving the gas and the jet is $b = 0.098x$ where x is the distance downstream of the jet's entrance point. If no decay in jet centerline velocity were to be experienced at distance x, then the minimum jet width would have to be $w_j = 2b = 0.196x$. This means that, if centerline velocity decay is to be avoided across the aperture, where $x = 7.62$ cm, the required jet width must be 1.49 cm. Since the tunnel will be constantly replenished by the inert gas under normal operating conditions, it is not absolutely necessary that this centerline velocity decay be avoided. Therefore, the jet width can be less than 1.49 cm as far as mixing with the tunnel gas is concerned. It should be noted that the preceding length to diameter ratio ($x/w_j = 5.1$), where centerline velocity decay begins, is valid for a wide range of jet velocities and is well substantiated by experimental data as shown in Fig. 2.2 of Ref. 5.

A more crucial aspect is the jet mixing with the laser gas. This mixing region as defined by Eq. (23.30) of Ref. 4 is

$$u = \frac{U_1 + U_2}{2}\left[1 + \left(\frac{U_1 - U_2}{U_1 + U_2}\right)\mathrm{erf}\left(\frac{13.5y}{x}\right)\right] \tag{5}$$

In this expression u is the velocity at a distance y from the line bisecting the mixing region; U_1 is the larger laser gas velocity; U_2 is the smaller jet velocity; and x is the distance from the jet entrance point. An average value of U_1 over the aperture region was calculated from Eqs. (1-3). Assuming a helium jet with a temperature T_j equal to the laser gas temperature at the nozzle exit plane, an assumed value of $U_2 = U_1/2$ represents a high subsonic value for M_j. With this value of U_2 and $x = 7.62$ cm, negative values of y were selected to determine the depth within the jet where $u/U_2 = 1.0$. It was found, for example, that at $y \cong -0.72$ cm, this velocity ratio is $u/U_2 \cong 1.028$.

A second analysis of the mixing region between the laser gas and the jet was made using a computer program known as BLAZE-III.[3] This program which is similar in structure to BLAZE-IV has a specific application to viscous flows. Assuming the same velocity and temperatures for the two streams as used in the preceding analysis, the diffusion boundary of the laser gas within the jet was calculated using this program. This boundary, using the previous definition of velocity ratio, represents a velocity ratio $u/U_2 = 1.0$. The results indicated a diffusion depth of $d = 0.72$ cm at $x = 7.62$ cm. This shows good agreement with the result using the Schlichting expression since the two velocity ratios (1.028 and 1.0) are very nearly equal at the same lateral distance ($d = |y| = 0.72$ cm).

An outer boundary of the laser gas was estimated by adding to the lateral displacement at each axial point on the calculated gas streamline of Fig. 3 a diffusion depth which is proportional to the axial distance from the jet entrance point. The result is shown as curve 3 in Fig. 3 when $p_t = p_e$ and as a boundary terminating at point P_3 in Fig. 4 when $p_t < p_e$.

The diffusion depth of 0.72 cm for the laser gas suggested that the jet width should be twice this value or 1.44 cm if the jet was to act effectively as a curtain. It was decided to select a slightly smaller jet width of 1.27 cm (0.5 in.), since the jet spreading on the tunnel side of the jet will have a beneficial effect of providing additional jet width.

Hydraulic Analogy

There is an analogy between a gas flow and the flow of shallow water with a free surface. Developed by Preiswerk[6] and known as the hydraulic analogy, it permits a simple, inexpensive means of observing gas flow phenomena which might otherwise be difficult to examine or, if observable,

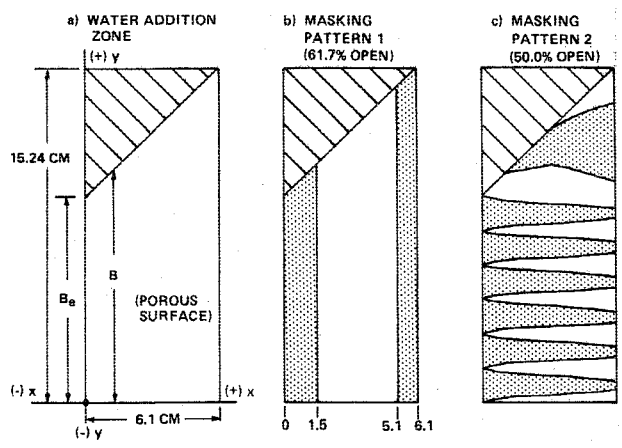

Fig. 5 Water addition zone and masking patterns.

might require expensive gas flow testing. The analog test device known as a water table lends itself readily to our problem of determining the merits of the containment device by using a water simulation of the laser gas and the jet curtain flow in the aperture region.

From the generalized one-dimensional flow equations of Ref. 7, the variation in Mach number with area and total temperature is

$$\frac{dM^2}{M^2} = \frac{-2\{1+[(\gamma-1)/2]M^2\}}{(1-M^2)}\frac{dA}{A} + \frac{(1+\gamma M^2)\{1+[(\gamma-1)/2]M^2\}}{(1-M^2)}\frac{dT_0}{T_0} \tag{6}$$

A corresponding equation for the variation in static pressure with area and total temperature when combined with Eq. (6) to eliminate the temperature effect gives

$$\frac{dp}{p} = -\frac{\gamma M^2}{1+\gamma M^2}\left[\frac{dM^2}{M^2}+\frac{dA}{A}\right] \tag{7}$$

Equations (6) and (7) are the basic gas flow equations as far as the hydraulic analogy is concerned.

Consider now an open channel whose horizontal bottom surface is parallel to the xy plane of Fig. 1 and whose variable width B increases in the positive y direction. Shallow water of variable depth H flows in the positive x direction. Applying the x-direction momentum equation to this flow, expanding and neglecting higher-order terms, and using the definition of Froude number which is $F=V(gH)^{-1/2}$ one obtains

$$\frac{dH^2}{H^2} = -\frac{2F^2}{1+2F^2}\left[\frac{dF^2}{F^2}+\frac{dB}{B}\right] \tag{8}$$

Using this equation in conjunction with the continuity equation yields

$$\frac{dF^2}{F^2} = -\frac{2(1+F^2/2)}{(1-F^2)}\frac{dB}{B} + \frac{2(1+2F^2)}{(1-F^2)}\frac{d\dot{w}}{\dot{w}} \tag{9}$$

where $\dot{w}$ denotes water flow rate. It should be noted that the last term in this equation differs from that in Eq. (5.5-8) of Ref. 1 which is in error.

Comparison of Eq. (7) with its water counterpart, Eq. (8), shows that with $\gamma=2$ there is a one-to-one correspondence between terms involving p and H^2, M^2, and F^2, and A and B. Therefore, water flow represents the flow of a gas with a $\gamma=2$. Because γ cannot exceed 1.67 for a gas, the water simulation is not exact.

Equation (9) is the water counterpart of Eq. (6), and the last terms in these equations show that the temperature increase in the laser cavity can be represented by water addition (secondary flow) to the primary flow representing the laser gas entering the cavity. This is true only if the water is added at the same speed and in the same direction as the primary flow. This is an ideal type of injection which is impossible to achieve in practice. A more realistic and practical approach is the normal injection of water through the bottom surface of the channel, as was done in Ref. 1 and this study. If Eqs. (8) and (9) are to retain their validity for this type of an injection, then the water must be added in a manner that permits the computed variation in water addition to be satisfied over large portions of the primary flowfield. In addition, the normal momentum of the secondary flow must be small so as not to significantly disturb the primary flow. Both requirements could be satisfied for small secondary flows using a porous injection surface of variable porosity. However, the second requirement can never be met if the secondary flow is a large fraction of the primary. It was therefore important to compute the required amount of water addition under ideal injection conditions to determine whether or not the gas temperature rise could be simulated.

In duplicating the gas temperature rise on the water table, one must set $dH^2/H^2=dp/p$ and $dB/B=dA/A$. Then, from Eqs. (7) and (8) it is seen that $dF^2/F^2=dM^2/M^2$. With variations in F^2 and B known, the total amount of water to be added for a temperature increase can be computed from Eq. (9). Using Eqs. (1-4) along with the laser width and laser cavity height y_w variation shown in Fig. 1, the secondary flow rate required to simulate the gas temperature rise was calculated to be 46.8% of the primary. This large secondary flow requirement ruled out any possibility of simulating the temperature rise in our problem.

An alternative to simulating the temperature rise is the injection of only that amount of water required to match the gas static pressure rise with a corresponding water depth profile on the water table. This profile was determined by setting the gradient of the square of the water depth equal to the gradient of the static pressure as defined by Eq. (4). Integrating and noting that at $x=0$, $H=H_g$ gave

$$H/H_g = (1.0-0.015x)^{1/2} \qquad (0.0<x\leq 1.5) \tag{10a}$$

$$H/H_g = (0.584+0.262x)^{1/2} \qquad (1.5<x\leq 5.1) \tag{10b}$$

$$H/H_g = (1.997-0.015x)^{1/2} \qquad (5.1<x\leq 6.1) \tag{10c}$$

Satisfying Eq. (10) on the water table insures matching the gas static pressure gradient without having to simulate the total temperature rise that produced it.

The term H_g in Eq. (10) is the raised height of the gate on the side of the primary flow reservoir and represents the depth of the primary water entering the channel. Laitone[8] notes that, if the surface wave velocity $c=(gH)^{1/2}$ as used in the definition of the Froude number is to be constant and independent of surface wavelength as assumed in the development of the water equations, then the water depth must be approximately 0.635 cm. Selecting the incoming water depth H_g as 0.635 cm, the required water depth profile was calculated from Eq. (10).

Design Requirements

The previous analyses provided the basis for establishing requirements relating to the design of the water table. Each of these is discussed in the following paragraphs.

A basic consideration in the design was that the channel be sized to permit full-scale testing of the DF laser shown in Fig. 1. Only one side of the laser needed examination since identical expanding flow conditions exist on both sides. Specifying the maximum channel width to be the same as the laser cavity width, then using the dimensional data of Fig. 1 and noting that $dB/B=dA/A$ gave an expression for channel width which is

$$B/B_e = 1.0+0.103x \tag{11}$$

where subscript e denotes the channel entrance. Assuming that the channel attains its full width at the end of the heat addition zone ($x=6.1$ cm), the entrance width was found to be $B_e=9.36$ cm.

The required primary flow rate $\dot{w}_p$ was computed in terms of the channel entrance conditions from

$$\dot{w}=\rho F_e(gH_g)^{1/2}A_e \tag{12}$$

where ρ, g, and A_e are water density, gravitational constant, and entrance area, respectively. With $F_e=M_e=3.8$, and $A_e=B_eH_g$, the primary flow rate was calculated to be 563.6 g/s (33.8 liters/min).

The secondary flow rate $\dot{w}_s$ was unknown at this point. However, it was known that its injection would have to

produce the water depth profile as defined by Eq. (10). In order to do this, it was necessary to inject the flow through a uniformly porous surface and obtain the depth profile by proper masking of the surface. Figure 5a shows this surface in the xy plane of Fig. 1 where the gas expansion takes place at the lower side of this figure in the $-y$ direction. The triangular cross-hatched region is a nonflow region representing the variable channel width defined by Eq. (11).

Two different masking patterns were constructed. Pattern 1, which is shown in Fig. 5b, blocks off the two areas xB where x varies from 0 to 1.5 cm and from 5.1 to 6.1 cm. This is equivalent to establishing the near constant water depths of 0.635 cm and 0.88 cm in these two regions of x as expressed by Eqs. (10a) and (10c), while permitting a linear addition of water between $x=1.5$ cm and $x=5.1$ cm. This pattern, which leaves 61.7% of the porous surface unmasked, was expected to give a good approximation to the depth profile in the flow direction plus provide a uniform injection in the lateral direction.

Pattern 2, which is shown in Fig. 5c, was computed analytically assuming ideal injection conditions and a simulation of the gas temperature rise. Although not shown here, the development consisted of computing the contour of several identical masking strips in the rectangular region and a single one in the triangular region. The contours were obtained by specifying the percentage of the surface to be masked, the number of masking strips in the rectangular region, and then satisfying the axial gradient of the previously computed secondary flow rate. With 50.0% masking and six strips, the pattern shown was expected to duplicate the desired water depth profile. Because of its finite number of strips it was not expected to provide uniformity of injection in the lateral direction.

The jet curtain flow rate $\dot{w}_j$ on the table was computed assuming a gaseous helium jet in the laser operating at a condition of $p_j=p_e$. Since the turbulent mixing zone approaches zero when $U_2 \rightarrow U_1$ [see Eq. (5)], then by attempting to match the average velocity in the jet with the average laser gas velocity over the aperture region, one is assured that the previously selected value of $\dot{w}_j = 1.27$ cm will be more than an adequate width for the jet. Picking values of M_j from 1.0 to 8.0, the required jet temperatures for velocity matching were found to vary from 2400 K to 620 K, respectively. By selecting jet widths of 0.635 cm and 1.27 cm and the preceding values of M_j, the jet curtain water flow rate on the table was calculated using Eq. (12) with $F_j=M_j$, $H_j=H_g$, and $A_j=\dot{w}_j H_j$. It was found to vary from a minimum of 10.1 g/s (0.6 liters/min) to a maximum of 161.0 g/s (9.66 liters/min).

Experimental

The experimental phase was divided into two parts. These were the design and fabrication of the water table and the testing.

Design and Fabrication

The most important aspect of this effort was the design of a reservoir system for both the primary and secondary flow since these systems must provide a smooth, relatively nonturbulent, mixed flow in the test section which is representative of the flow in the laser cavity. Figure 6 shows pictorially these systems relative to the table surface (xy plane). The primary flow enters vertically into settling chamber 1, passes through a perforated circular tube at the bottom, and then into the chamber itself which is partially filled with 0.25-cm diameter ceramic beads (shaded area). The perforated tube and the beads have the effect of eliminating the large-scale turbulence of the entering flow. The primary flow then passes through the screen partition separating compartments 1 and 2 and then through a folded screen insert at the bottom of chamber 2. Passage through these screen surfaces eliminated the remaining flow turbulence so that the flow entering the

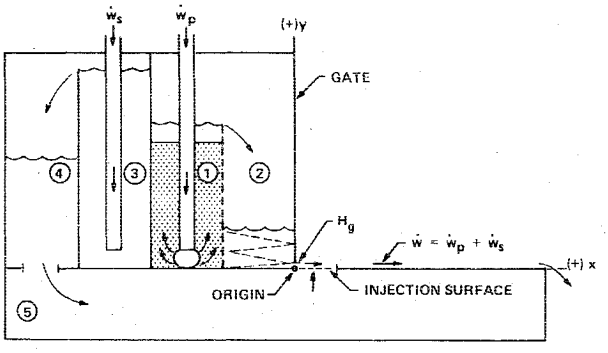

Fig. 6 Primary and secondary flow reservoir systems.

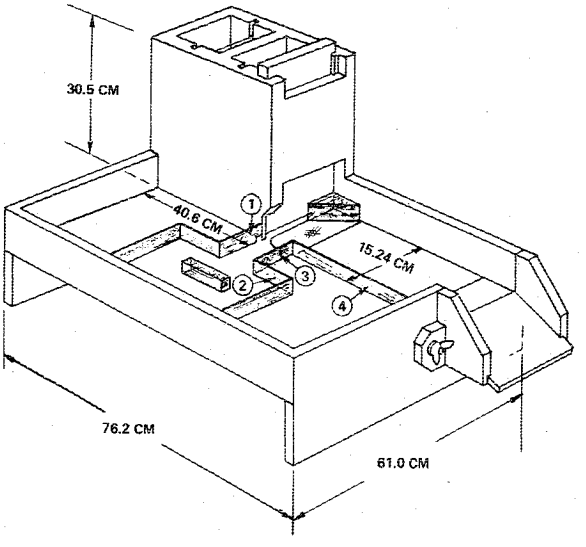

Fig. 7 Sketch of the water table.

water channel from underneath the vertically raised gate was of excellent quality.

The secondary flow enters vertically into settling chamber 3, and spills over a solid wall into a second settling chamber 4. From there the water flows into a large plenum chamber 5 located underneath the table surface by way of two large holes in the bottom of chamber 4. Flow of this water through the porous injection surface insures that it too will be of good quality. The material chosen for the porous injection surface was a wire mesh laminate known as Dynapore which has a pressure drop of 0.35 N/cm^2 at a flow of 1.76 liters/min-cm.[2]

Figure 7 shows a sketch of the assembled all-plexiglas water table. With the width of each of the four upright compartments equal to that of the 15.24-cm channel, the 61.0-cm (24-in.) width of the table was established by the requirement that the full-scale optical system must be accommodated on its surface. The 76.2-cm (30-in.) length was somewhat arbitrary in that having specified the 40.6-cm (16-in.) base dimension for the upright compartments, it provided what seemed to be an adequate flow length beyond the aperture opening so that disturbances created by flow impinging upon the end wall of the table would not greatly influence the flow within the region of the aperture.

The walls of the optical cavity system, the simulated mirror located wihin the optical cavity, and the triangular corner block, all shown shaded, were also fabricated from plexiglas. The triangular block and a rectangular block within the primary reservoir form an integral unit intended to provide better water flow entrance conditions on the reservoir side of the gate and the desired channel width variation on the downstream side.

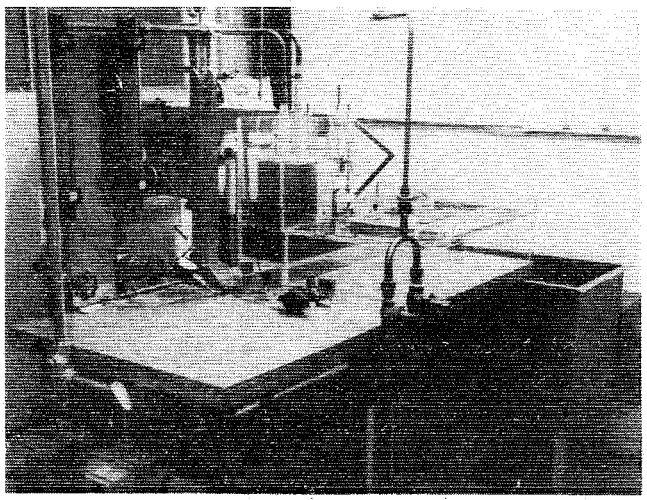

Fig. 8 Installed water table.

Tunnel wall 1 was designed with a notch in the bottom corner adjacent to the outside wall of the primary flow reservoir to accommodate the jet nozzle to be located there. Although not shown here, the tunnel walls 2 and 3 and the cavity wall 4 have adjustable lengths permitting variation in the aperture and a displacement of the cavity wall up to 4.45 cm.

Three plexiglas jet nozzles were fabricated, all with exit heights of 0.635 cm. Known as nozzles A, B, and C, nozzles A and C were 0.635-cm wide while nozzle B was 1.27-cm wide. Electrical conduit putty was used to reshape the internal flow passage of nozzle C so that its exit height would more nearly match the pressure in the tunnel entrance.

Figure 8 shows the plexiglas water table installed on a 0.76×1.52m (2.5×5.0 ft) table with the catch tank shown at the far end. The two switch boxes shown in the foreground are for the primary and secondary water pumps which were mounted on the floor. These identical centrifugal pumps, which have a maximum pumping capability of 75.7 liters/min, provide a recirculating system by pumping the collected water in the catch tank back into the upright compartments 1 and 3.

Two identical flow meters with a 100% flow capacity of 41.6 liters/min are mounted above the table and measure the primary and secondary flow rates. The two mounted on the front of the table have 100% flow capacities of 1.0 liter/min and 9.2 liters/min and measure the jet nozzle flow rate. The jet nozzle is shown attached to the wall of compartment 2 with a bracket that insures a flush mount of the nozzle against the outer wall.

Shown near the top of the picture is a Hardinge mill mounted on the floor behind the table. Mounted on its three-axis (x,y,z) movement platform is an arm extending out and over the flowing water and supporting a small steel rod on which was mounted a small Exacto knife blade. Water depth measurements at a given x,y location were made by lowering the point of the blade until contact was made with the water surface and the channel bottom and reading the differences between the two readings on the vertical scale as water depth.

A hand bulb pressure fed ink supply is shown on the left side of the table. It fed ink into the primary flow by way of a small feed line which passes approximately along the x axis and through compartments 4, 3, and 1 of Fig. 6 and into compartment 2 terminating very close to the origin shown there. Injection of ink at this point permitted the observation of the outer boundary of this flow over the aperture region.

Testing

Prior to actual testing, it was determined that masking pattern 2 provided the best match of the water depth profile as defined by Eq. (10). Using this pattern, the required secondary flow rate was found to be 61.4 g/s (3.68 liters/min). This is 10.9% of the primary flow rate.

With both the primary and secondary flow rates known, the first test was to determine the lateral expansion of the simulated laser gas as represented by these combined flows. This test was conducted without the optical cavity configuration of Fig. 7 and after the water flowing onto the table surface had reached a depth which was constant and approximately equal to the height (H_g) of the entering primary flow. This represented, as nearly as possible, the $p_t = p_e$ condition which was assumed in the calculation of the water streamline.

The expansion of the simulated gas was determined with the aid of a grid marked on masking tape and attached to the table surface at the aperture location. Ink was injected on the ambient water surface just outside of the anticipated outer streamline location using a hand-held hypodermic needle. The outer streamline location was determined as the locus of points where the ink-identified aspiration-induced flow patterns were destroyed by the fast moving primary flow.

The second test was the determination of the outer boundary of the simulated laser gas using the optical cavity configuration shown in Fig. 7. This was done by injecting ink into the primary flow and establishing the location of the boundary using the grid just described.

The remainder of the tests were also conducted using the optical cavity configuration of Fig. 7. They consisted of determining for a given jet nozzle and wall displacement, the minimum jet Froude number and flow rate that would effectively prevent the simulated laser gas flow from entering the tunnel.

Results

The observed outer streamline of the simulated laser gas is shown as curve 4 in Fig. 3. It shows reasonably good agreement with the analytical prediction (curve 2) when one considers the approximations made in the calculation of the contour, the rather simple manner in which this streamline was determined, and the fact that true ambient conditions are not achieved by a finite size test facility.

The observed outer boundary of the simulated laser gas is shown as curve 5 in Fig. 3. As expected, it shows a greater lateral displacement than the estimated boundary (curve 3) since p_t was less than p_e in the test. In addition, this boundary was found to be virtually independent of wall displacement. Drawn to scale in Fig. 4, where it terminates at point P_3, it shows that if all the laser gas is to be captured, then the minimum value of Δ must equal the lateral displacement of point P_3 which is about 2.0 cm. If Δ equals or exceeds the lateral displacement of point P_2, then the entire jet flow will be captured as well.

The minimum jet Froude number required to contain the simulated laser gas is shown plotted as a function of wall displacement for each of the three nozzles in the upper set of curves in Fig. 9. Since these are minimum values of F_j, the regions above each curve represents all values of F_j which will effectively prevent the simulated laser gas from entering the tunnel. A comparison of nozzles A and B, which have the same height h_j, shows that the wider one (B) is more efficient as a barrier since it contains the simulated laser flow with a much lower momentum (lower F_j). This was postulated as being the result of the greater integrity of the wider jet when subjected to the destructive action of diffusion. A comparison of nozzles A and C, which have the same width, shows that the taller one (A) is more efficient. Here, the greater expansion of the flow emanating from nozzle A is apparently beneficial.

Each of the upper set of curves in Fig. 9 exhibits a minimum point at wall displacements ranging from about 2.6 cm to 3.2 cm. Noting these minimum points by their wall displacements (Δ_{min}), they can best be visualized in terms of the flow pattern

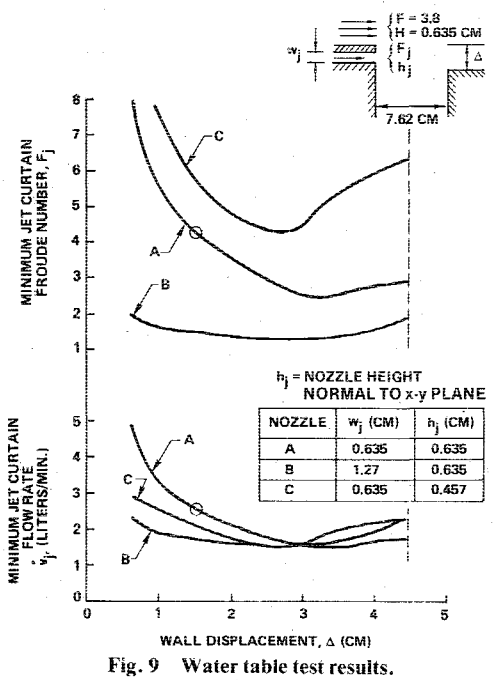

Fig. 9 Water table test results.

of Fig. 4. As noted previously, the wall displacement corresponding to point P_3 is about 2.0 cm. Points P_1 and P_2, which are also shown to scale, are observed jet boundary points for nozzle A and the wall displacement (3.18 cm) shown here. Detected on the water surface as regions of large velocity gradients, these points were found to be dependent upon Δ but independent of F_j. From Fig. 4, one sees that the wall displacement corresponding to point P_2 is about 2.5 cm when $\dot{w}_j = 0.635$ cm. If $\dot{w}_j = 1.27$ cm, then this wall displacement would be expected to be about 3.2 cm. These displacements, which are essentially the same as the foregoing range of Δ, suggest that when $\Delta = \Delta_{min}$ for a given nozzle, essentially all of the simulated laser gas flow and jet curtain flow is being captured as a result of the wall displacement.

The contour of each of the curves in the upper set of curves in Fig. 9 can be logically explained in the following manner: When Δ decreases below the value Δ_{min} for a given nozzle, a point is reached where point P_3 will intersect the corner of the cavity wall and the tunnel wall. A further decrease in wall displacement requires a jet of greater momentum to forcibly deflect the simulated laser gas around this corner. Furthermore, this required jet momentum will increase more rapidly as Δ continues to decrease. On the other hand, when Δ increases above the value of Δ_{min}, the simulated laser gas will impinge, divide, and turn at some point on the cavity wall downstream of the corner. The result is that a small portion of it will flow upstream through the cavity wall boundary layer toward the tunnel entrance. This reverse flow can be overcome by a low-momentum jet. However, since this reverse flow increases with wall displacement, the required jet momentum will now increase with increasing values of wall displacement.

The lower set of curves in Fig. 9 are a replot of the data in the upper set in which minimum jet curtain Froude number has been replaced by the minimum volumetric jet curtain flow rate $\dot{v}_j$. Again, since these are minimum values, the regions above each curve represent flow rates which will effectively prevent the simulated laser gas from entering the tunnel. These results show that minimum flow rate for a given nozzle occurs when $\Delta = \Delta_{min}$ and that this flow rate of 1.5 liters/min, which is the same for all nozzles, is only 4% of the simulated laser gas flow rate.

From the standpoint of jet flow requirements, one would conclude that the ideal wall displacement would be Δ_{min}. There are other considerations that enter into this choice.

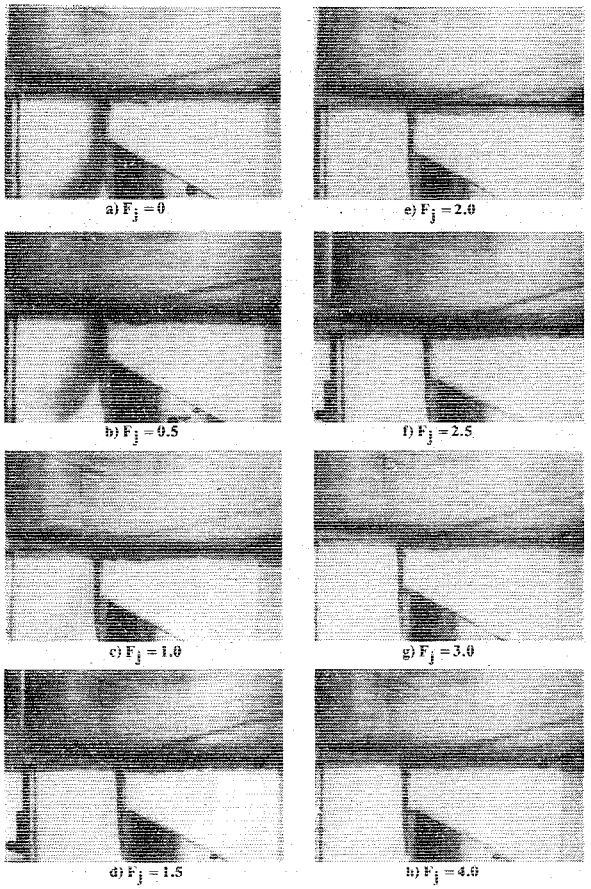

Fig. 10 Simulated flows in the aperture region. Nozzle A, Δ = 1.52 cm.

First of all, when $\Delta < \Delta_{min}$, the simulated laser gas is not permitted to expand freely. The jet, in turning the gas around the corner, creates disturbances within the interior region of the gas, and, as observed from the tests, these disturbances (hydraulic jumps) become more severe as the displacement decreases. The counterparts of these disturbances in the gas phase are shocks which result in a loss of output power from the laser. Secondly, when $\Delta > \Delta_{min}$, one worsens the problem of pressure recovery downstream of the laser cavity as displacement increases. Consequently, $\Delta = \Delta_{min}$ represents an ideal wall displacement.

Figure 10 shows photographs of the flow in the aperture region for nozzle A when $\Delta = 1.52$ cm. It corresponds to the circled points on the nozzle A curves of Fig. 9. For no jet flow, Fig. 10a shows a large ingestion of ink-darkened simulated laser gas entering the tunnel. Figures 10b-10h, with jet flow, show a steady decrease in this ingestion as the Froude number is increased. This increase is evident up to a value of $F_j = 2.0$ beyond which ingestion is still present in very small quantities although undetectable from the pictures. As shown in Fig. 9, this ingestion would be expected to continue until $F_j = 4.25$.

The results of Figs. 9 and 10 illustrate the effectiveness of the jet curtain on the water table and in doing so demonstrate its potential effectiveness in the corresponding gas flow case. It is important to remember that these results are a qualitative rather than a quantitative confirmation because of the difference between the value of γ for the gas and its equivalent value in water.

Conclusions

Through the use of the hydraulic analogy we have demonstrated the feasibility of jet curtains in a passive containment of a laser cavity gas when used in conjunction with a cavity wall displacement. Based upon the limited

results of examining a particular flow situation within a DF laser, the following additional conclusions can be made:

1) The ideal wall displacement for a given jet nozzle is the displacement (Δ_{min}) where the jet exit Froude number for containment is at a minimum.

2) In containing the laser gas with a displacement $\Delta = \Delta_{min}$, one is assured of a complete capture of the laser gas and a major part of the jet, a minimum jet flow rate, and a shock-free flow in the laser cavity.

Acknowledgment

The author wishes to thank G. Rudinger for his assistance in the design of the water table.

References

[1] Addy, A. L. and Mikkelsen, C. D., "An Investigation of Gas-Dynamic Flow Problems in Chemical Laser Systems," Gas Dynamic Laboratory, University of Illinois, UILU-Eng-74-4009, Dec. 1974.

[2] Parmentier, E. M. and Greenberg, R. A., "Supersonic Flow Aerodynamic Windows for High-Power Lasers," *AIAA Journal*, Vol. 11, July 1973, pp. 943-949.

[3] Zelazny, S. W. and Rushmore, W. L., "The Effect of Mixing Rate on Pressure Fields in Confined Flows," AIAA Paper 77-221, Jan. 1977.

[4] Schlichting, H., *Boundary Layer Theory*, McGraw-Hill, New York, 1960, pp. 590-599.

[5] Harsha, P. T., "Free Turbulent Mixing: A Critical Evaluation of Theory and Experiment," Arnold Engineering Development Center, Tenn., AEDC-TR-71-36, Feb. 1971.

[6] Preiswerk, E., "Application of the Methods of Gas Dynamics to Water Flows with Free Surface," NACA TM 934 and 935, March 1940.

[7] Shapiro, A. H., *The Dynamics and Thermodynamics of Compressible Fluid Flow*, Vol. 1, Ronald Press, 1953, Chap. 8.

[8] Laitone, E. V., "A Study of Transonic Gas Dynamics by the Hydraulic Analogy," *Journal of the Aeronautical Sciences*, Vol. 19, April 1952, pp. 265-272.